

Application of RFSoC Technology for Beam Position Monitors at the SuperKEKB Storage Rings Injection Points

B. Urbschat,^{a,b,1} **G. Mitsuka**,^{b,c} **L. Ruckman**^d

^a*Nagoya University,
Furo-Cho, Chikusa, Nagoya, Aichi, Japan*

^b*KEK,
Oho, Tsukuba, Ibaraki 305-0801, Japan*

^c*SOKENDAI,
Shonan Village, Hayama, Kanagawa 240-0193, Japan*

^d*SLAC National Accelerator Laboratory,
2575 Sand Hill Road, M/S 96, Menlo Park, CA 94025, USA*

E-mail: urbsch@hepl.phys.nagoya-u.ac.jp

ABSTRACT: In order to achieve its ambitious luminosity target, the SuperKEKB collider must achieve and sustain high beam currents on the order of Ampere in its storage rings. This requires continuous top-up injection and operation with a two-bunch injection scheme, injecting two 96 ns spaced bunches in a single injection cycle. An important input for tuning the injection beam is the position reading from a dedicated beam position monitor (BPM), located after the septum magnets, slightly upstream of where the injected and stored beams converge. Previously, the readout electronics used for these special BPMs were not capable of independent measurement of both bunches in the two-bunch injection mode and modification of the concerned devices and their firmware was not feasible. The opportunity was taken to develop a new readout device based on the AMD/Xilinx RF System on a Chip (RFSoC) platform with the goal of not only providing a sufficiently flexible and performant readout solution for the concerned BPMs, but also to evaluate and gain experience with the platform for beam monitor electronics applications. This paper is concerned with the details of this development as well as evaluation and operation of the developed device.

KEYWORDS: Beam-line instrumentation (beam position and profile monitors, beam-intensity monitors, bunch length monitors); Instrumentation for particle accelerators and storage rings - high energy (linear accelerators, synchrotrons); Data acquisition circuits

¹Corresponding author.

Contents

1	Motivation and Requirements	1
2	Hardware	2
2.1	SuperKEKB injection point BPM vacuum chamber	2
2.2	RFSoC 4x2 evaluation board	4
2.3	Analog circuit and signal conditioning	8
3	Firmware and Software	9
4	Evaluation and Operation	10
4.1	Resolution estimation at the KEK injector linac	10
4.2	Gain calibration	12
4.3	Use during SuperKEKB operations	15
5	Summary and Prospects	15
6	Acknowledgments	16

1 Motivation and Requirements

The SuperKEKB collider [1] is an electron-positron collider located at the High Energy Research Organization (KEK), Tsukuba, Japan. At the time of writing, SuperKEKB already holds the world record for highest instantaneous luminosity at $5.1 \times 10^{34} \text{ cm}^{-2} \text{ s}^{-1}$. However, in order to support the physics goals of the accompanying Belle II experiment [2], luminosities much beyond this value are demanded.

Operation at such high luminosities requires considerable beam currents on the order of multiple Ampere. This, combined with the rather short beam life on the order of tens of minutes necessitates efficient, continuous (top-up) injection into both of the collider’s storage rings. The injection frequency is however limited by the present infrastructure to maximally 25 Hz.

As a means to maximize injected charge given such limitations, a *two-bunch injection mode* was implemented [3]. During two-bunch injection, two 96 ns spaced bunches are accelerated during the same cycle of the injector linac and injected into two appropriately spaced bunches in either of the storage rings. This scheme effectively doubles the injected charge of around 2 nC for the electron beam and around 3 nC for the positron beam to twice as much per injection cycle.

To optimize injection efficiency (amount of stored charge compared to injected charge) the parameters of the injection (septum and kicker magnets) must be tuned. As an input to the tuning a special beam position monitor (BPM) located just upstream of the injection point is used to monitor the trajectory of the injected bunches. Notably the trajectories of both bunches in two-bunch injection mode may differ and must therefore be tuned separately. This of course necessitates

separate measurement of both trajectories while taking care to ensure independent measurements, meaning no overlap of signals from the first and second bunch, which would distort measurements. The present commercial BPM readout electronics were found to provide insufficient flexibility for this rather special application, leading us to pursue the in-house developed solution presented here.

The in-house development is further motivated by a general interest in adoption of the *RF System on a Chip* (RFSoC) platform by AMD/Xilinx [4] as a flexible solution for future beam monitor electronics, especially considering the excellent performance of the included analog-to-digital converters (ADCs) paired with the possibility for rapid development thanks to the single-chip adaptive solution.

In the following, we first provide an overview of the used hardware spanning the BPM vacuum chamber as well as the adopted method for position calculation, used 3rd generation RFSoC evaluation board and analog frontend circuit. As part of the introduction of the RFSoC evaluation board, a measurement of the effective number of bits of the 3rd generation RFSoC's ADCs measured using that board is presented. Next, we provide a high level overview of the custom firmware and software developed for our application. The following section focuses on evaluation of the developed readout device and its use during accelerator operations. We present results of an early resolution estimation study conducted at the KEK injector linac during the development phase, address necessary channel gain corrections as well as give a summary of use during recent SuperKEKB operations. We conclude with a short summary and prospects for future developments of the application concerned by this paper as well as RFSoC based electronics for beam monitors at KEK in general.

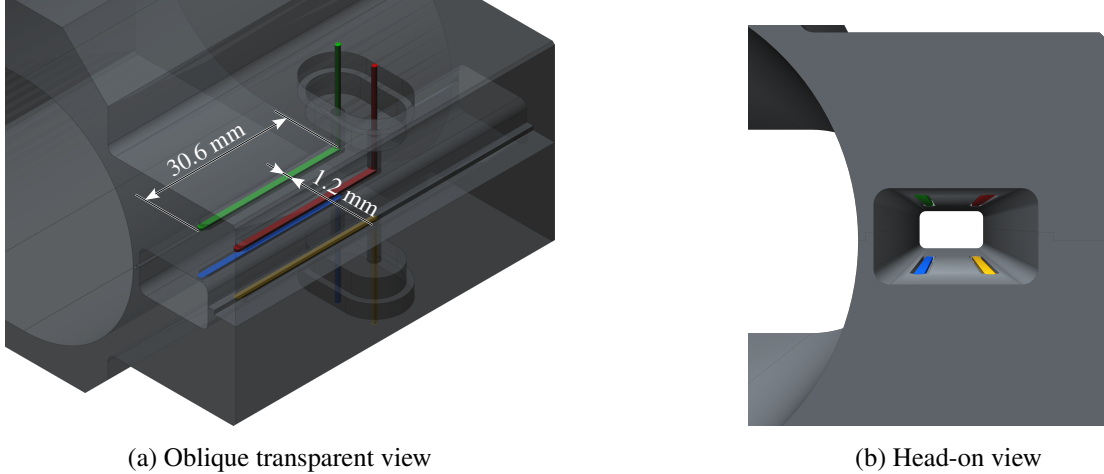
2 Hardware

2.1 SuperKEKB injection point BPM vacuum chamber

Both the electron and the positron ring of SuperKEKB feature a special *injection point BPM*, measuring the trajectory of the injection beams just upstream of the injection point where storage and injection beam vacuum chambers converge and the injection beam meets the storage beam. As shown in figure 1, the injection beam duct is attached to the side of the storage beam's chamber as at the location of the BPM injection and storage beam are already brought into close proximity. Four pickup electrodes of stripline type, shorted to the chamber's body at one end and connected to a feedthrough at the other, are placed at the top and bottom of the injection beam duct.

The injection beam duct is rather small, sized 8 mm \times 15 mm for the electron ring and 8 mm \times 16.6 mm for the positron ring and the beam does not necessarily traverse it near its center. Given the rectangular geometry and rather wide range of possible beam positions, it is not feasible to analytically derive a relationship between the signals from the electrodes and beam position.

Alternatively a map of signal strengths as a function of beam position may be obtained in discrete form, either experimentally (by stretched wire scan) or by adequate simulation. The discrete map can then be interpolated wherever a continuous one is required. As no stretched wire scan of the chambers was performed before installation, we are forced to rely on results from simulation. Specifically a custom simulation code based on the Boundary Element Method (BEM) in two dimensions is used. Due to the nature of this simulation only the signal strength in arbitrary



(a) Oblique transparent view

(b) Head-on view

Figure 1: Simplified 3D model of the injection point BPM vacuum chamber for the electron ring.

units but *not* the shape of the signal waveform is determined. The signal strength is assumed to be proportional to the integral of the absolute values of the digitized waveforms. An absolute scale is not required for position measurement. It would be a requirement for an absolute charge measurement, however in our application a relative measure of bunch charge suffices.

The obtained signal maps with overlaid chamber cross-sections for both rings are shown in figure 2. The electrodes are modeled as a section of the chamber wall. In reality, while the electrodes do sit flush with the chamber wall, there is a small gap on their sides and back to isolate them from the chamber wall. Considering manufacturing tolerances and other factors, it was deemed unnecessary to model fine details like the small gaps, as they are likely to not exactly represent reality to begin with. This does however lead to disagreements between simulated and true signal response, which become significant for beam positions near the electrodes as further discussed in section 4.2.

Note that the chamber geometries slightly differ between electron and positron ring. The positron ring's chamber is of an older type where the electrodes were arranged asymmetrically in an attempt to improve sensitivity near the edges of the chamber. During recent operations this was not found to provide any advantage and rather only introduce unnecessary complications. Thus, the electron ring's chamber was already exchanged for a new one with symmetric electrode arrangement. As the new chamber geometry was found to work well, the same will be installed for the positron ring in the future.

The signal maps form the base for computation of the beam position as a function of the four signal strengths from the four electrodes. It was attempted to approximate this relationship using polynomials in four variables (the signal strengths), one for each direction in the plane. While this is expected to work well for beam positions near the center of the duct, for the full range of expected beam positions in our application, even with polynomials of very high degree (12 and above), only unsatisfactory results could be achieved.

Thus, instead an iterative algorithm is adopted to find the position coordinates x, y for which the signal strengths determined by simulation are closest to the measured ones. The coordinates x, y are determined such that the quantity $f(x, y)$ as defined in eq. (2.1) is minimal. $s_i^{\text{map}}(x, y)$ is the signal strength for the i -th electrode obtained for a given position x, y from the interpolated signal

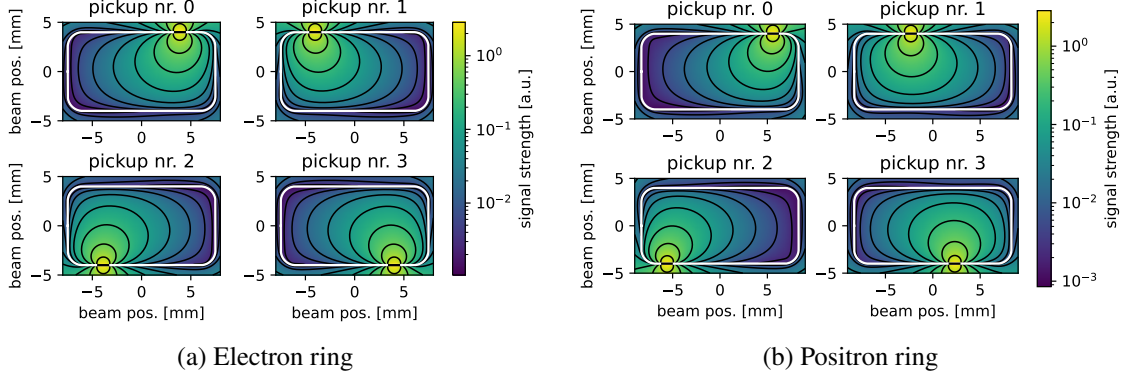


Figure 2: Signal maps for all electrodes of the used BPM chambers as determined by BEM simulation. The used chamber outline is shown in white. Only the map values within the outline are of relevance. Black lines represent logarithmically spaced contours.

strength map. s_i is the measured signal strength for the i -th electrode.

$$f(x, y) = \sum_{i=0}^3 \left(\frac{s_i^{\text{map}}(x, y)}{\sum_{i=0}^3 s_i^{\text{map}}(x, y)} - \frac{s_i}{\sum_{i=0}^3 s_i} \right)^2. \quad (2.1)$$

For the minimization a C++ implementation of the *BOBYQA* algorithm [5, 6] is used. This algorithm runs sufficiently fast to meet the 25 Hz injection rate requirement with ease.

Finally, it shall be noted that due to the placement of the used BPM chamber, a meaningful in-situ assessment of the resolution by the 3-BPM [7] method is difficult, as one would have to reliably determine and reflect the effect of the septum magnets located between the injection point BPM and other BPMs located further upstream.

While not directly comparable, an estimation of resolution when using the developed readout was carried out at the KEK injector linac, using the BPM chambers installed there. Results from this study are presented in section 4.1.

2.2 RFSoC 4x2 evaluation board

An *RFSoC 4x2* evaluation board designed and distributed by RealDigital is used to read out the signals from the BPM's pickups. This board features a 3rd generation RFSoC containing high performance ADCs and digital-to-analog converters (DACs), ARM processors as well as an FPGA fabric united in a single package. The used evaluation board provides access to four of the integrated 14-bit, 5 GSPS ADCs and two of its 14-bit, 9.85 GSPS DACs. Further inputs are available for trigger and clock signals. A photograph of the board is shown in figure 3.

Effective Number of Bits For our application the *effective number of bits* (ENOB) of the ADCs, a measure of the actual resolution of an ADC, is an important performance metric. I. Degl'Innocenti et al. report an ENOB of around 9.5 in their survey of recent ADCs [8], which is extracted from the device's datasheet. We are not aware of any publications verifying the ADC performance by measurement of the ENOB (or equivalent measurement) for a 3rd generation RFSoC. The ADCs for the 3rd generation are 14-bit ADCs while previous generations had 12-bit ADCs. Especially for

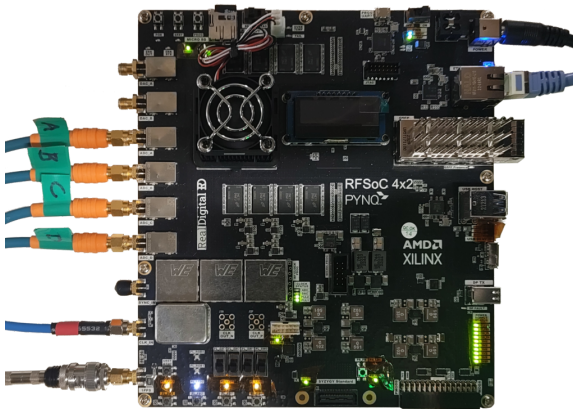


Figure 3: Photograph of the used RFSoC 4x2 evaluation board.

the 1st generation chips some detailed evaluations have been published [9]. Given the lack of an independent verification of the ADCs performance, we decided to conduct an ENOB measurement using the RFSoC 4x2 board. The ENOB is computed from the *signal-to-noise and distortion ratio* (SINAD) as described in [10]. SINAD captures the dynamic performance of an ADC as the ratio of a single tone's power (signal power) to the power in the remaining spectrum, however excluding DC (sum of noise and distortion power). We convert SINAD to ENOB as that allows for a more intuitive interpretation.

An Agilent E8663D signal generator as well as bandpass filters had to be employed to achieve sufficiently clean single tones. Without the bandpass filters the measurement was strongly influenced by noise and distortion from the signal generator, leading to measured ENOB of up to two bits lower than what was measured with the filters. Further, even with bandpass filters in place, some noise may leak through which still can have an influence on the measurement. Initially an Agilent N5181B was used which however had a high enough noise floor for frequencies below around 300 MHz to significantly degrade the measured ENOB.

Bandpass filters were available for 150 MHz (Mini-Circuits *SBP-150+*), 1.5 GHz and 2 GHz (custom coupled stripline). Signal power is set so as to achieve the largest possible signal at the ADCs which is still within their input range. For the bandpass filters at 1.5 GHz and 2 GHz the insertion loss was very large and even at the maximum output power of the signal generators of 18 dBm only around a third of the ADCs input range could be used. This however does not directly pose a problem as in the analysis the power of each tone is measured relative to the full ADC scale and appropriate scaling is applied. The ADC sampling clock is locked to the 10 MHz reference signal of the signal generator by configuring the dedicated PLLs on the RFSoC 4x2 board accordingly. The ADC sampling frequency is chosen as 4.072 GHz, an integer multiple of 509 MHz, which is close to the SuperKEKB global RF clock frequency the board will eventually reference during operation. The number of samples in a buffer is chosen as 8144, which divides the sampling rate. Measurements then may be taken at the frequencies $f_n = n \cdot 4.072 \text{ GHz} / 8144$ where $n = 1, 2, 3, \dots$ and $f_n < 2 \text{ GHz}$. This condition ensures a whole number of cycles of the sampled sinusoidal signal in the buffer, thus eliminating the need for windowing functions for the discrete Fourier transform. Windowing the signal has an effect on its power spectrum, which would

have to be corrected. By using a setup which does not require windowing in the first place, such complications are circumvented.

In order to assess statistical fluctuations, the measurement is repeated 50 times at each frequency and for each channel. The mean over the 50 measurements with one standard deviation as the uncertainty for each channel is presented in table 1.

Table 1: ENOB measurements for the 3rd generation RFSoC ADCs in each of the four channels (A, B, C, D) available on the RFSoC 4x2 board.

Frequency	Filter	ENOB			
		A	B	C	D
150 MHz	SBP-150	10.08 ± 0.02	10.00 ± 0.01	10.06 ± 0.01	9.97 ± 0.02
1.5 GHz	coupled stripline	10.16 ± 0.01	10.07 ± 0.02	10.11 ± 0.01	10.03 ± 0.01
2 GHz	coupled stripline	10.05 ± 0.02	9.96 ± 0.02	10.04 ± 0.02	9.95 ± 0.02

Degl’Innocenti et. al. [8] use the performance metric $P = 2^{\text{ENOB}} \cdot f_s$ to compare different ADCs based on values extracted from corresponding datasheets. The input signal frequency is chosen as close as possible to half of the maximum sampling rate f_s . The best ADCs score a value of around $P_{\text{best}} = 2.90 \times 10^{12} \text{ s}^{-1}$. Our measurement for an input signal near 2 GHz implies around $P \approx 4.2 \times 10^{12} \text{ s}^{-1}$ computed with $f_s = 4.072 \text{ GHz}$ which is the sampling frequency for our setup.

The measured ENOB values and resulting performance metrics even slightly exceed the values suggested by the datasheet. This confirms that the 3rd RFSoC ADCs are indeed performing excellently and represent the state of the art of ADC technology.

Digital Step Attenuators The 3rd generation RFSoCs, as used on the RFSoC 4x2 board, include *digital step attenuators* (DSAs) in each analog signal path providing 0 dB to 27 dB attenuation adjustable in 1 dB steps. Although not yet implemented, we explored the possibility to employ the DSAs to dynamically set the attenuation for each signal channel independently to optimize utilization of the ADCs dynamic range. This is especially interesting in our use case where the beam is likely to traverse the BPM chamber off-center, leading to a large asymmetry in the signal amplitudes. For this however it is vital to understand the characteristics of each attenuator in order to correct for possible differences between the set and true attenuation.

A simple scan of attenuation values over the available range showed that the set attenuations appear to be accurate to within about 1 dB. Figure 4 shows the difference between measured and expected power (up to a constant offset) as a function of the set attenuation in each channel available on the RFSoC 4x2 board, measured at 200 MHz and 1.5 GHz¹. A constant offset remains as in the calculation we reference 0 dBFS (decibels relative to full scale) but the input signal did not actually fill the whole ADC range. It is the same for all four channels as the signal power was not changed between measurements. The measurements were performed with a sinusoidal input signal and the power is extracted from the discrete Fourier transform of the recorded signal using the same procedure (clock synchronization, buffer size) as used for the ENOB measurement presented above. Power at the signal generator was set to 4.80 dBm.

¹Further frequencies were checked, but are not shown in figure 4 to avoid clutter.

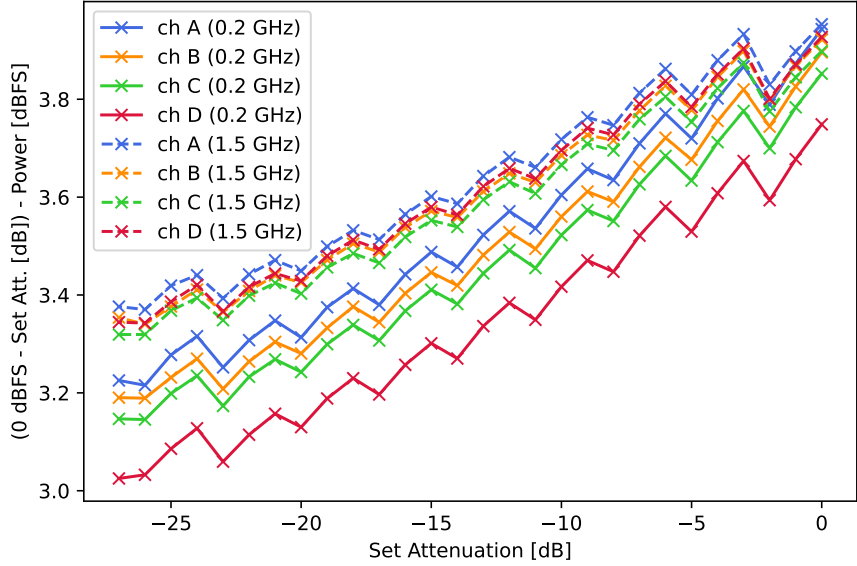


Figure 4: Difference between expected and measured signal power (up to a constant offset) as a function of the set attenuation of the step attenuator in each of the four channels available on an RFSoC 4x2 evaluation board.

Clearly there are some relative offsets on the order of tenths of a decibel between the four channels. This may be attributed to slight differences in the signal path, which could also be related to the signal traces on the printed circuit board. Interestingly, up to an offset, at a given frequency the curves in all four channels take almost exactly the same shape. This indicates good relative accuracy between the attenuation elements used in the step attenuator of a given channel. A sawtooth-like pattern is observed, repeating every three decibels (i.e. every three steps). This is likely related to a given attenuation element being switched in or out of the signal path. The period of three rather than a power of two further suggests that the step attenuator is likely to be a little more sophisticated than a simple series of switched 2^n dB ($n = 0, 1, 2, \dots$) attenuation elements, which also would not fit in with the maximum attenuation of 27 dB.

While a very similar pattern appears when measuring at different frequencies, the relative offsets do exhibit frequency dependence. Further, the overall slope towards lower attenuations appears ever so slightly shallower for the higher frequencies. This means that while a frequency dependence exists, it is for the most part independent of the attenuator setting. In any case, this can in principle be corrected for. If further the sampled signal does only change in amplitude but its spectral composition remains constant, the corrections are much simpler, as in this case the corrections can be applied directly in the time domain, while in general they may have to be applied in the frequency domain. In our application, the signal bandwidth is well defined and narrow enough to make corrections in only the time domain sufficient.

Further, given the observed relative offsets even at fixed frequency, it is clear that in our application, if attenuation is set separately in each channel, the attenuators must be properly characterized in order to apply attenuation value dependent compensation. If however attenuators in all four channels are set to the same value (and constant offsets between channels are accounted for), an

attenuation value dependent compensation may be safely omitted.

2.3 Analog circuit and signal conditioning

The signal as obtained from the pickup electrodes is a rather short (~ 2 ns) broadband pulse as shown in figure 5. When digitizing this signal in its raw state, only very few samples can be acquired. Further, especially the samples on the steep rising edge are highly sensitive to slight variations in signal timing as may be introduced by for example thermal influences on the transmission lines. This poses a problem for long-term stability of the beam position measurements. This effect was observed during a study using the KEK injector linac, the details of which are described in section 4.1 (a). Therefore, in order to maximize the number of samples acquired and mitigate above mentioned effects, the signal is conditioned such as to stretch it as much as possible. The upper limit for signal length is given by the 96 ns spacing of both bunches in two-bunch injection mode, as the signal from first and second bunch may not overlap.

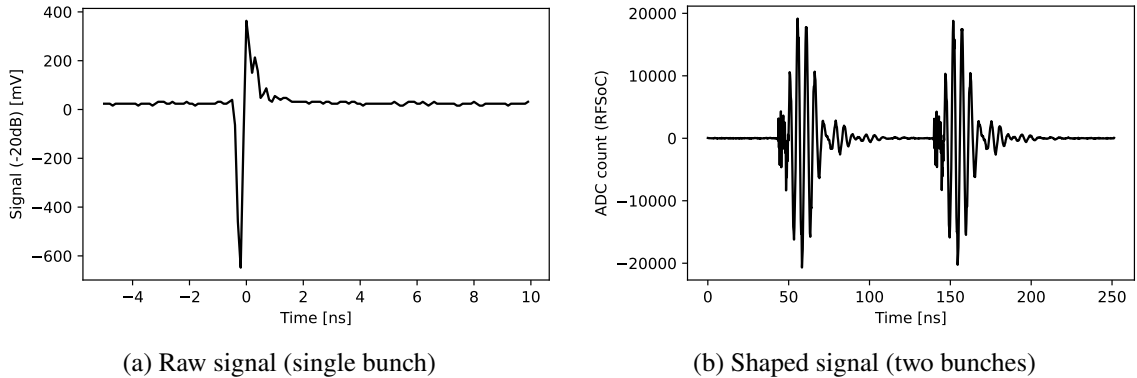


Figure 5: Raw and shaped waveform from one of the electrodes. The former is attenuated by 20 dB and captured using a Rohde&Schwarz *RTO 1024*, 10 GSPS oscilloscope. The latter is captured using the RFSoC 4x2 board. Note the large difference in time scales.

Stretching of the signal can be achieved by limiting its bandwidth by means of a bandpass filter. The bandwidth is approximately inversely proportional to the signal length and thus can be tuned by selecting a suitable bandpass filter. While custom, optimized filters may be prepared eventually, for current operation commercially available filters by Mini-Circuits are used. A survey based on the S-parameter data published by Mini-Circuits showed that a *SBP-150+* bandpass or a combination of a *SHP-200+* (highpass) and *SLP-200+* (lowpass) filters may provide suitable signal conditioning. Initially four of each were purchased for testing. When testing with actual signals during beam operation, the *SBP-150+* turned out to produce a shaped signal slightly longer than the 96 ns between injected bunches, leading us to adopt the combination of *SHP-200+* and *SLP-200+*, which fulfilled the spacing requirement.

Due to the filters, the signal is attenuated to a few tens of millivolts peak-to-peak. Thus, to optimally utilize the input range of the ADCs, a MITEQ *AFS2-00100400-15-10P-4* +20 dB amplifier is inserted into the signal path of each channel, after the filters. This amplifier was chosen as it not only fulfills or even exceeds the required specifications but also was simply already available in sufficient quantity, leftover from a previous project.

The shaped signal (i.e. with filters and amplifier inserted) for the case of two-bunch injection is shown in figure 5 (b). Note that the timescale is different from the raw signal by more than an order of magnitude. As the signal was recorded with the RFSoC 4x2 board, the y-axis shows ADC counts rather than voltage. Evidently the stretching of the signal is close to what is possible within the constraint given by the 96 ns bunch spacing.

3 Firmware and Software

The firmware run on the RFSoC uses the *axi-soc-ultra-plus-core* framework developed at SLAC [11]. A block diagram of the firmware is shown in figure 6. The *RF Data Converter* (RFDC) is the hardware block included in the RFSoC chip containing the ADCs and DACs. It exposes RF inputs and outputs, a sampling clock input as well as an interface to the FPGA, referred to in the following as the Programmable Logic (PL). We lock the RFDC sampling clock to the global RF clock of SuperKEKB at 508.89 MHz. The ADCs and DACs sampling frequency is an integer multiple of this frequency. The sampling frequency is chosen as the highest possible one satisfying this condition which is 4.065 GHz. While the DACs are not directly required for our application, we include functionality to replay arbitrary waveforms in the firmware which is convenient for testing purposes, e.g. loopback of DAC outputs into ADC inputs.

Data from the four available ADCs is continuously streamed to ring buffers implemented in the PL. Ring buffers of two different sizes are available. The larger one is sized at around 2 μ s and may be read out for debugging and monitoring purposes at a slow rate (usually around 1 Hz) if requested by software. The smaller one is sized at around 300 ns which is sufficient for a recording of signals from both bunches in two-bunch injection mode, including some margin. Readout of this buffer is triggered by the injection trigger signal received from accelerator controls at maximally 25 Hz (although the firmware in principle may support much higher trigger rates). A suitable delay is applied to the trigger in the firmware.

The CPU, here referred to as the Processing System (PS), runs an embedded Linux distribution build using the Yocto Project tools. Data from the ring buffers is streamed to the PS via Direct Memory Access (DMA). For access to firmware registers a second interface is available mapping the registers into the Linux memory space. Stream DMA as well as register access use dedicated Linux kernel drivers [12].

As illustrated in figure 7, a TCP bridge application is run in Linux userspace extending the stream and register interfaces over the local network. This utilizes the *rogue* framework [13] developed at SLAC, providing an abstraction of the interfaces and high level access using Python and/or C++. Firmware control and waveform processing is handled by a rogue-based application run on a rack server with all communication traversing the TCP bridge. There is no restriction on the machine such an application may be run on as long as it is connected to the same network as the RFSoC board, allowing for a flexible development flow. In principle the application can also be run on the RFSoC's embedded CPU, which however may lack the performance required for some more computationally heavy tasks. Some processing may also be implemented in PL, which however is not necessary for our application with relatively low trigger rate.

The rack server application handles setup of the RFSoC board through the register interface as well as processing of the incoming waveform data for each injection. The absolute value of the

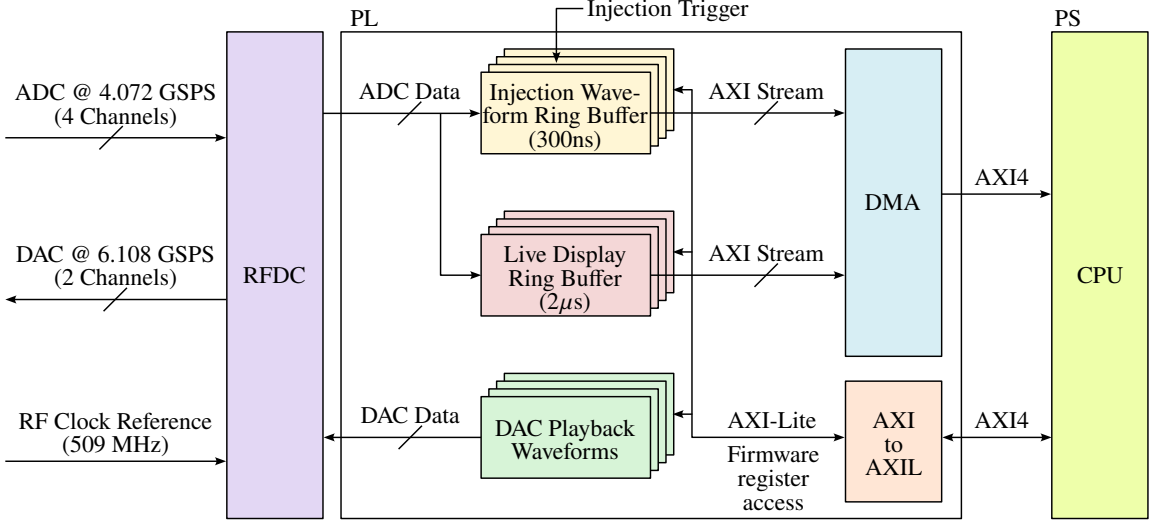


Figure 6: Block diagram of the firmware run on the RFSoC.

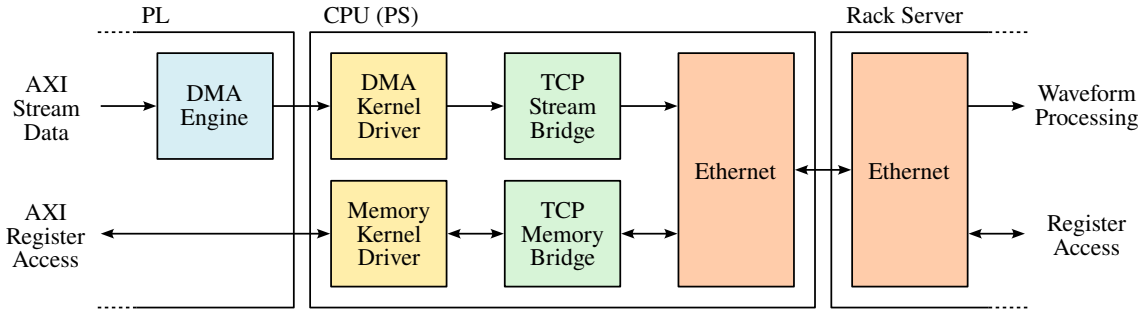


Figure 7: Block diagram of the TCP bridge used for data transfer between the RFSoC board and a rack server running the waveform processing and device control code.

signal is integrated in a set time window for each injected bunch. The obtained integral values are used as the signal strengths s_i and position is computed by minimizing eq. (2.1) as described in section 2.1. While the control code is implemented in Python, the used minimizer is implemented in C++ and invoked from Python code to ensure sufficiently fast execution.

4 Evaluation and Operation

4.1 Resolution estimation at the KEK injector linac

In order to verify basic operation and feasibility of the developed device, a resolution study at the KEK injector linac was conducted during its operation in June 2025. This study used the stripline BPM chambers installed at the linac, which are, as opposed to the SuperKEKB injection point BPMs, of much simpler geometry (cylindrical with symmetric electrode arrangement). Thus the pickup characteristics are expected to be quite different. While the results of this study cannot be directly translated to the injection point BPM chamber, they still are useful to judge whether

performance of the RFSoC based readout electronics is sufficient by comparing with the resolution achieved by the readout electronics currently installed at the linac [14].

During the study the importance of signal conditioning was not yet established and no proper bandpass filters were available. However, to still somewhat stretch the signal eventually *Mini-Circuits SLP-450* lowpass filters were added to the setup.

As only one RFSoC 4x2 board was available at the time, a resolution measurement using the ordinary 3-BPM method [7], where three identical setups are prepared and data is analyzed under the assumption that the resolution of all setups is identical, was not possible. Instead, data from two BPMs using the linac readout electronics was combined with the data from a third one, located downstream from the other two, read out using the RFSoC 4x2 board. In this setup the assumption of equal resolutions is obviously not adequate. Therefore the resolution for a BPM with linac readout electronics had to be determined separately using the ordinary 3-BPM method first, to then use it in the resolution estimation for the RFSoC based readout. For the 3-BPM measurement we used data from the same two BPMs as used for the RFSoC readout resolution estimation, complemented by a third one located upstream of the other two.

To ensure a fair comparison, the data used for both the estimation of resolution with linac BPM readout electronics as well as with the RFSoC based readout electronics was taken from the same time window. The beam position was scanned for around 1.5 mm in the vertical (y) direction over the course of 25 minutes. In both cases the resolution is determined from the width of the distribution of differences between estimated and measured position at the third, most downstream BPM. The estimated position is determined by using the measured positions y_1, y_2 at the two upstream BPMs to linearly extrapolate the downstream beam position as $y_3 = Ay_1 + By_2 + C$. The constants A, B and C are determined by a fit over all available data. For the fit to properly converge a range of positions is required. Thus only the data for the vertical direction where the sweep was performed is used. The estimated and measured positions as well as the distribution of their differences are shown in figure 8. The resolution is extracted from the standard deviation of the distribution of differences. For the case of only linac BPM readout electronics this is done under the assumption of equal resolutions for all three setups (figure 8, left) resulting in $\sigma_{\text{linac}} = 8.6 \mu\text{m}$. For the measurement of the RFSoC based readout, this resolution is then propagated through the linear extrapolation and eventually subtracted in quadrature from the standard deviation of the corresponding distribution (figure 8, right), resulting in $\sigma_{\text{rfsoc}} = 8.7 \mu\text{m}$.

The obtained resolution for the RFSoC based readout is within our expectations of at least 10 μm . Further it is comparable to the resolution achieved by the linac readout electronics under the operating conditions during the study. It shall be noted that the linac BPMs paired with their readout electronics may be capable of resolutions down to 4 μm [14], which however is known to depend on operating conditions, thus rendering the observed resolution of 8.6 μm still realistic. Further, in terms of raw ADC performance, the RFSoC should outperform the linac readout electronics but nevertheless did not achieve a resolution superior to the latter. This however can be explained by the lack of proper signal conditioning for the RFSoC based readout. The linac readout electronics contain carefully tuned, purpose-built bandpass filters to condition the signal in order to maximize the number of samples per pulse by stretching it as much as possible within the limit of 96 ns between bunches. The lowpass filters used for the RFSoC based readout only stretched the signal to around 20 ns at best. If proper signal conditioning is applied, around 4.5 times more samples can

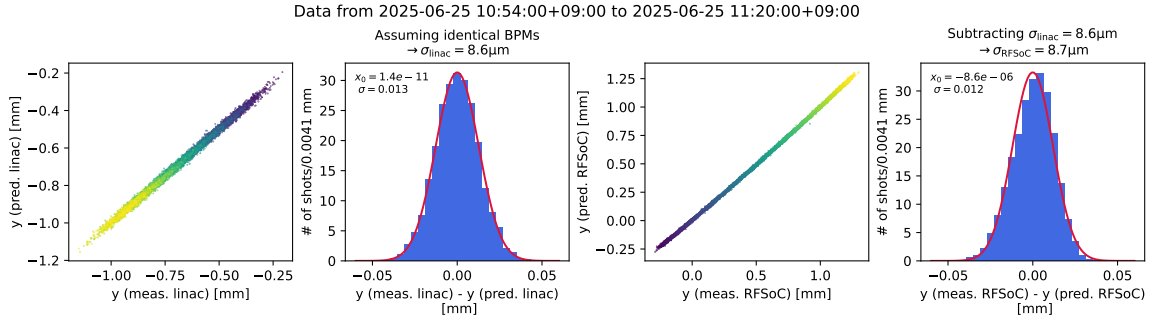


Figure 8: Predicted and measured vertical beam position used for resolution estimation. Due to the combination of RFSoC based and present linac readout electronics used, the resolution for the latter is determined first (left) and used in the resolution calculation of the former (right).

be acquired, which should improve the resolution simply by statistical advantage.

A further artifact of the improper signal conditioning is the slight skew in the distribution shown in figure 8 (right). The short signal and resulting lack of statistics combined with the rather steep edges of the waveform make the position measurements sensitive to even very small variations in relative phase of the signals from the electrodes (likely influenced by temperature of the transmission lines, connectors etc.). The result is a small drift of the position measurement becoming quite noticeable when measuring for longer than around 30 minutes. This effect was later reproduced on the bench, replaying signals of different shapes using the DACs and confirmed to be negligible if proper signal conditioning is applied. However, it is clear that direct digitization of the raw broadband pulse is not an option as for a BPM application, where long term stability of the measurement is essential.

4.2 Gain calibration

A number of factors, including differences introduced by cables, filters etc., may influence the gain of each of the four channels. As all those factors are difficult to evaluate separately, a beam data-driven method is employed to correct for the resulting overall gain differences at once.

We leverage on the fact that fit-based position computation method as described in section 2.1 in principle also works with only three out of the four available electrodes. One may simply exclude the signal from one of the four electrodes from the minimized function presented in eq. (2.1). Excluding a signal is in the following referred to as *masking* it. There exist four masks masking exactly one of the four channels. If the overall gain for each channel is exactly the same, the four positions computed with each of the four masks (in an ideal scenario) match exactly. However, in the case of relative differences in channel gain, the four positions will no longer match. Therefore, in the case of real (non idealized) data, the spread among the four positions is expected to assume a minimum when the gain of each channel is corrected such as to eliminate any relative gain differences between channels.

To quantify the spread among the four positions computed with the four masks we use the quantity r , defined as described in the following. Let g_i where $i = 0, 1, 2, 3$ be the correction factor applied to the signal from the i -th channel to obtain the corrected signal $s_i = g_i \cdot s_i^{\text{raw}}$ used as an input to the position computation described in section 2.1. We compute (as a function of the g_i) for

each shot (index j) and direction ($d = x, y$) the variance $\sigma_{d,j}^2(\{g_i\})$ over the four values obtained with the four masks. For N shots this yields $2N$ values, which are then summed to obtain the quantity r , which is to be minimized.

$$r(\{g_i\}) = \frac{1}{2N} \sum_{d=x,y} \sum_{j=0}^{N-1} \sigma_{d,j}^2(\{g_i\}). \quad (4.1)$$

The g_i minimizing this function are taken as the gain correction factors.

In practice, this minimization turned out to be non-trivial. The dependence on the position computation, being itself based on a minimization procedure using a rather complex signal strength map as an input, makes the minimized quantity r a considerably complex function of the gain correction factors g_i . This significantly increases the chance for the minimization to fail or get stuck in a local minimum. Such behavior was observed for all attempted minimizers, even on idealized (generated) data. To circumvent this, we first manually tune initial values for the g_i , judging the spread of the positions computed with the masks by eye, by means of a simple scatter plot. Using the such determined initial values, a minimizer is usually able to find the correct global minimum. The choice of minimizer did not matter much if initial values are chosen carefully. We settled on the *scipy* [15] implementation of the *Nelder-Mead* method. As the problem only has three degrees of freedom, we fix $g_0 = 1$ and vary only the remaining three parameters.

Further complications arise when using real data recorded during accelerator operation. First, during normal operations the injected beam usually traverses the injection point BPM at around the same position, dictated by the trajectory required for successful injection. Thus, the available data usually only covers a small range (around a millimeter of spread) of positions. Studies using idealized data showed that significant biases may be picked up when the covered range of positions is this small.

To avoid this, a dedicated study was conducted where the injection beam was manually steered over an as large as possible range by manually adjusting the septum magnets located directly upstream of the BPM. There is no beam shutter located downstream of the injection point BPMs, so during the study, the injected beam inevitably enters the SuperKEKB storage rings. As the trajectory of the injected beam is adjusted to far beyond what is used during normal operations, the injected charge is unlikely to enter a stable trajectory in the ring. This in turn may lead to beam losses in the ring exceeding the thresholds set for a beam abort and thus must be avoided. By conducting the study just after the start of the 2026 SuperKEKB operations, where the rings were still operated with detuned optics and collimator settings, providing a large acceptance for the injected beam, as well as reducing the charge per injection and disabling one of the injection kickers in the ring, losses could be suppressed sufficiently.

The study was conducted for both of the electron and positron beams. Results for both beams are similar, although the region where satisfactory accuracy could be achieved was much smaller for the positron beam. This is understood to be related to the different electrode arrangement in the BPM chamber. For beam positions very close to the electrodes, the four positions computed with masks tend to spread out further, independent of the chosen set of gain correction factors, indicating disagreement between simulation and true signal response, as mentioned in section 2.1. For the positron beam, the electrode arrangement appears to amplify this effect. As the case of the electron

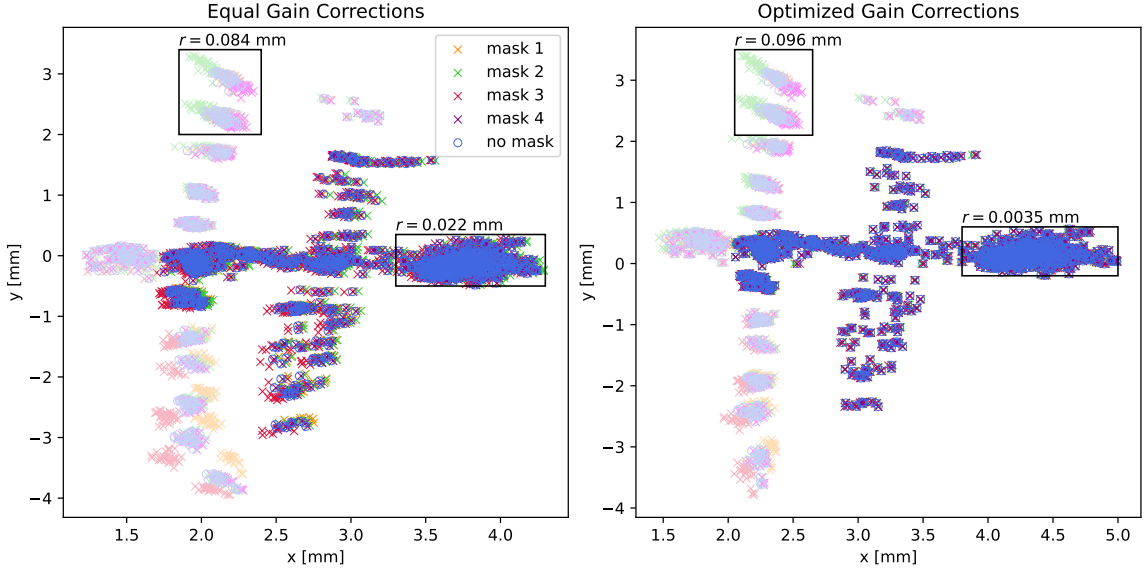


Figure 9: Beam positions recorded during the gain correction study, computed with each of the four possible masks as well as without any mask. Points excluded from the minimization of r are shown in a lighter shade. Shown values of r are computed over the regions indicated in black.

beam better illustrates our method and further the chamber for the positron beam is scheduled to be replaced with a new one of the same geometry as the one currently used for the electron beam anyways², we restrict the following discussion to the case of the electron beam.

The beam positions recorded during the study, computed with each mask as well as without mask, for the case of equal gain correction factors (equivalent to no gain correction applied) and optimized gain correction factors are shown in figure 9. For some regions, especially near the electrodes, it was found to be impossible to reduce the spread of positions computed with masks much further than what is shown for the case with optimized gain corrections. As this is understood to be a result of the discrepancy between BEM simulation and true signal responses, the data from those regions is excluded from the minimization process of r . The excluded points in figure 9 are plotted in lighter shades than those used for the minimization.

Figure 9 further indicates the value of r computed over two regions, one near one of the electrodes and the other near the usual location of the beam during operations, before and after the optimization. In the former, r does only slightly change (even increases) despite of a clear reduction of r in the latter. In this context, r may be considered a systematic uncertainty of the beam position. For the beam positions during normal operations, $r \approx 3.5 \mu\text{m}$, which is small compared with the usual jitter of the beam. Evidently gain compensation by the above presented method works well, as long as the beam is not steered too close to one of the electrodes.

²It is planned to perform a stretched wire scan of the new chamber at this opportunity to better assess uncertainties of the currently used BEM simulation.

4.3 Use during SuperKEKB operations

The readout electronics for both rings of SuperKEKB were switched over to the RFSoC based readout during the first weeks of the operational period starting in November 2025.

The determined beam positions are provided to accelerator controls through the *Experimental Physics and Industrial Control System* (EPICS) so called *process variables* (PVs) published using *pythonSoftIOC* [16], which was integrated into the server side application. A much larger number of variables is exposed through the rogue framework and can be accessed over the local network.

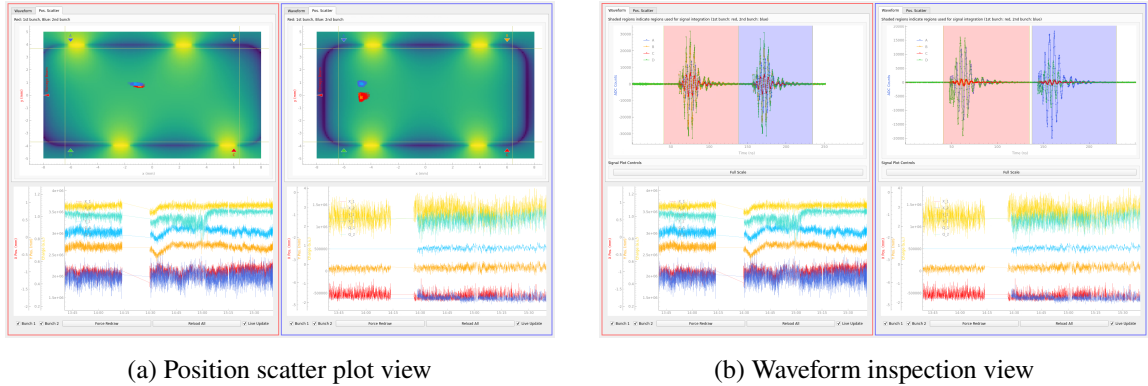


Figure 10: Screenshots of the GUI prepared for the control room.

A graphical user interface (GUI) or operator panel was prepared for use in the SuperKEKB control room. This panel is based on *pydm* [17] and fetches information from both EPICS PVs as well as rogue remote variables. Screenshots of the panel are shown in figure 10. A *scatter plot* tab, where the beam positions are plotted in near real time, as well as a *waveform* tab to inspect the raw waveforms is available. The former is plotted on top of the BEM map data summed over all four channels to give some visual indication of the sensitivity of each electrode for a given beam position as well as indicate the boundary of the beam duct.

As no major complications have been encountered during the operations so far, the initially temporary setup was moved to a proper rack mounted enclosure for permanent installation during the 2025/2026 winter shutdown. The final configuration is shown in figure 11

5 Summary and Prospects

In order to achieve its luminosity goals, SuperKEKB must sustain high beam currents, which in turn requires continuous top-up injection. To maximize the injected charge, tuning of the injection beam is required, an important input to which is the position reading from the injection point BPMs. We developed and successfully deployed a flexible solution for reliable position measurement, specifically capable of independent measurement of both bunches in the two-bunch injection mode, which with the previously used readout device was only possible to a limited extent.

We adopted the RFSoC platform for this development with the secondary goal of collecting experience with the technology towards future use for beam monitor readout electronics at KEK. The RFSoC platform in combination with the tooling and framework developed at SLAC was found



Figure 11: Photograph of the RFSoC 4x2 board, filters, amplifiers and power supply in the final configuration installed in a rack mounted enclosure.

to provide a solid foundation enabling efficient and flexible development of application specific, high performance readout solutions involving RF sampling.

Studies towards possible adoption of RFSoC based readout at the *beam transport* line, connecting the injector linac to the SuperKEKB storage rings, are already underway. As part of this, further features are being added to the firmware, including integration with an event timing distribution system over optical fiber as well as dynamic attenuator adjustment using the digital step attenuators available in the 3rd generation RFSoCs.

Possible applications for use with fast bunch-by-bunch synchrotron radiation monitors as well a large-scale deployment for a renewal of the readout electronics of a subset of the BPMs installed in the SuperKEKB storage rings, also involving a feedback system, are under consideration. For such applications, the currently used evaluation boards are no longer suitable, which is why for future developments adoption of an RFSoC *System on Module* (SoM) centered platform is planned.

6 Acknowledgments

The work of B. Urbschat and G. Mitsuka was supported by Japan Society for the Promotion of Science (JSPS) International Leading Research Grant Number JP22K21347. L. Ruckman's work was supported by the U.S. Department of Energy, under contract number DE-AC02-76SF00515.

We would further like to thank F. Miyahara (KEK injector linac controls/beam monitor group) and N. Iida (beam transport line group) for assisting with the resolution study and collection of calibration data respectively.

References

- [1] “SuperKEKB design report.” <https://kds.kek.jp/event/15914/>.
- [2] T. Abe, I. Adachi, K. Adamczyk, S. Ahn, H. Aihara, K. Akai et al., *Belle II technical design report*, Tech. Rep. KEK Report 2010-1 (2010), [DOI](#).
- [3] H. Sugimura et al., *Trigger control system with beam gate at SuperKEKB injector linac and damping ring*, in *Proc. PASJ’18*, no. 15 in PASJ’18 - 15th Annular Conference of the Particle Accelerator Society of Japan, pp. 1078–1081, 10, 2018, https://www.pasj.jp/web_publish/pasj2018/proceedings/PDF/THP0/THP091.pdf.
- [4] *White paper: An adaptable direct RF-sampling solution*, Tech. Rep. [WP489](#), AMD/Xilinx (2, 2019).
- [5] M.J. Powell et al., *The BOBYQA algorithm for bound constrained optimization without derivatives*, *Cambridge NA Report NA2009/06, University of Cambridge, Cambridge* **26** (2009) 26.
- [6] D. Pitzl, “Bounded optimization by quadratic optimization.” <https://github.com/pitzl/bobyqa/>, 2018.
- [7] M. Arinaga, J. Flanagan, S. Hiramatsu, T. Ieiri, H. Ikeda, H. Ishii et al., *Kekb beam instrumentation systems*, *Nuclear Instruments and Methods in Physics Research Section A: Accelerators, Spectrometers, Detectors and Associated Equipment* **499** (2003) 100.
- [8] I. Degl’Innocenti et al., *HL-LHC BPM electronics development as a case study for direct digitization and integrated processing techniques in accelerator instrumentation*, in *Proc. 14th International Particle Accelerator Conference*, no. 14 in IPAC’23 - 14th International Particle Accelerator Conference, pp. 4657–4660, JACoW Publishing, Geneva, Switzerland, 5, 2023, [DOI](#).
- [9] C. Liu, M.E. Jones and A.C. Taylor, *Characterizing the performance of high-speed data converters for RFSoC-based radio astronomy receivers*, *Monthly Notices of the Royal Astronomical Society* **501** (2020) 5096.
- [10] W. Kester, “Analog devices tutorial MT-003.” <https://www.analog.com/media/en/training-seminars/tutorials/MT-003.pdf>, 2009.
- [11] L. Ruckman, “slaclab/axi-soc-ultra-plus-core.” [Computer Software] <https://www.osti.gov/doecode/biblio/75773>, 8, 2021. 10.11578/dc.20220711.1.
- [12] B. Reese, L. Ruckman, R. Herbst and J. Pines, “aes-stream-drivers.” [Computer Software] <https://www.osti.gov/doecode/biblio/8043>.
- [13] J. Prudhomme, B. Reese, D. Doering, F. Abu-Nimeh, J. Vasquez, M. Kwiatkowski et al., “rogue.” [Computer Software] <https://www.osti.gov/doecode/biblio/8153>.
- [14] R. Ichimiya et al., *High position resolution and high dynamic range stripline beam position monitor (BPM) readout system for the KEKB injector linac towards the SuperKEKB*, in *Proc. IBIC’14*, no. 3 in IBIC’23 - 3rd International Beam Instrumentation Conference, pp. 637–641, JACoW Publishing, Geneva, Switzerland, 2014, <http://jacow.org/IBIC2014/papers/wepd04.pdf>.
- [15] P. Virtanen, R. Gommers, T.E. Oliphant, M. Haberland, T. Reddy, D. Cournapeau et al., *SciPy 1.0: Fundamental Algorithms for Scientific Computing in Python*, *Nature Methods* **17** (2020) 261.
- [16] “pythonsoftioc.” <https://github.com/DiamondLightSource/pythonSoftIOC>, 2025.
- [17] S. Alverson, G. Fedel, T. Rendahl, X. Resende, H. Slepicka, Z. Lentz et al., “Python display manager.” [Computer Software] <https://www.osti.gov/doecode/biblio/8121>.